Needle Deflection Prediction Using Adaptive Slope Model

Ederson Antônio Gomes Dorileô, Nabil Zemiti, Philippe Poignet

Needle Deflection Prediction Using Adaptive Slope Model

Éderson Dorileo, Nabil Zemiti, Philippe Poignet
Robotic Department - LIRMM
University of Montpellier
Montpellier, France
{Name.Surname}@lirmm.fr

***Abstract*—Thin and long (semi-rigid) needles are well known to bend during percutaneous insertions because of needle-tissue interactions. Robot-driven needle insertions have been proposed to improve the efficacy of procedures, such as radiofrequency ablation (RFA) of kidney tumors. However, the success of treatments and diagnosis depends on accurate prediction of needle deflection. This work aims to demonstrate the feasibility of merging needle-tissue properties, tip asymmetry and needle tip position updates to assist needle placement. The model design matches the observations of transversal and axial resultant forces acting in the system, while the slope parameter between them provides major contribution to the analysis of online and offline needle deflections predictions. Online updates of the needle tip position allow adaptive corrections of the slope parameter. Moreover, promising results were observed while evaluating the model´s performance under uncertainties conditions such as tissue deformation, tissue inhomogeneity, needle-tissue friction, topological changes of the tissue and other modeling approximations. The system is evaluated by experiments in soft (homogeneous) PVC and multilayer tissue phantoms. Experiment results of needle placement into soft tissues presented average error of 1.04 mm. Meanwhile, online corrections decreased the error of offline predictions of 25%. The system shows an encouraging ability to predict semi-rigid needle deflection during interactions with elastic medium.**

Keywords—percutaneous insertion; needle deflection prediction; modeling; adaptive slope model

I. INTRODUCTION

Image-guided needle insertion is a common interventional radiology act. Clinical applications such as radiofrequency ablation (RFA) of kidney tumors demand accurate needle placement, since errors during the percutaneous insertion can mitigate the effectiveness of the procedure.

Often, for simplicity's sake or environment´s constraints, the linear projection is taken as reference [1]. However, in real insertion scenario, the thin and long (semi-rigid) needles used tend to bend with a typical range of 50-90 mm [2]. System´s parameters such as tissue deformation, inhomogeneity, anisotropy or physiological movements (i.e. breathing) can increase the positioning errors by deviating the needle from its intended path. Moreover, tip asymmetry and other mechanical parameters of the needle seem to be strongly related to its deflection [3] [4] [5]. Robot-driven needle insertions have been proposed to improve the efficacy of percutaneous procedures. However, the success of treatments and diagnosis depends on accurate prediction of the needle deflection.

Over the last decade, needle deflection prediction approaches have been studied considering different experimental scenarios. These approaches have supported applications, such as needle's insertion point assistance, path planning and needle steering. Comparing deterministically these approaches is difficult because of the variations in the experimental puncture conditions. Needle steering methods using lateral needle motions outside the tissue were first devised by [6] and [7] in order to guide the needle through insertion into soft tissue. In the first work, DiMaio et al. proposed a method to predict needle motion, whose insertion was formulated as a trajectory planning and control problem. A manipulation Jacobian was defined using simulation models. Variations of the numerical needle insertion models were in the range of nearly 1mm to 2.5mm. The model designed in [7] assumed the needle as a linear beam supported by virtual springs, where the stiffness coefficients of the springs can vary along the needle. Forward and inverse kinematics of the needle were solved analytically, providing adaptive corrections for real-time (RT) fluoroscopic guidance. The approach was validated for flexible needles.

Recently, a number of experimental studies [8] [9] [10] [11] have proposed thin and flexible needle steering based on techniques such as duty cycling rotations [12]. The basic idea is to simultaneously insert and rotate the needle, while providing different needle curvatures during the insertion. It has been shown that needle rotation significantly decreases the puncture force [13] when compared to lateral needle motions. In addition, it could reduce the amount of tissue indentation as well as the friction force between the needle shaft and the tissue. However, according to [14], needle spinning methods don't solve the problem entirely due to the risk to patient safety and tissue damage. In contrast, there are also active researches on needle-tissue interaction modeling and robotic insertion preplanning aiming to improve targeting accuracy despite the bevel effect. In addition to the safety reasons, steering methods discussed in many previous works cannot be used in several of the aforementioned cases because of needle stiffness (RFA

This work was developed with support of the ANR (National Research Agency - France) in the context of the TECSAN project ROBACUS (ANR-11-TECS-020-01).

needle is not flexible when compared with nitinol needles). Moreover, in many percutaneous therapies, the needle has to be inserted along a straight path as it is constrained by the abdominal wall [15]. In such cases, the needle must be accurately directed to the target lesion once puncture occurs, since after puncture, the needle immediately advances inside the tissue. Therefore, it is important to make a correct analysis of needle deflection and set appropriate conditions in which the puncture occurs.

Some research groups have conducted studies in order to find the optimized insertion point and orientation using linear and nonlinear models [16] [17]. The neo-Hookean model developed by Dehghan et al. [16] considered geometric and mechanical non-linearities, as well as compressibility effects in simulations for prostate brachytherapy. The algorithm showed convergence in a few iterations, but the use of non-linear models is computationally expensive. The FEM-based algorithm proposed in [17] run comparatively faster using a linear model in the brachytherapy simulator. Experiments results presented in further works [18] [19] evaluated beam deflection modeled in the context of needle deflections predictions. Euler-Bernoulli cantilever beam theory was designed considering both: a) beam with free end load and b) beam supported by springs having needle-tissue interaction stiffness. The deflection models were developed aiming to be integrated in further applications of needle path planning and steering. For the first case [18], the friction force was found to be dependent on the insertion velocity and it was determined for needle inserted under controlled velocities. Errors were found to reach 2.3 mm into nonhomogenous tissue. The model´s design did not consider tissue´s stiffness during the experiments and neither considered any adaptive device to correct such approximation. Therefore, the experiment results may not be invariant to changes in the tissue´s properties, while potential over fit to the experimental conditions might not work under different scenarios. Further work integrated tissue´s properties in the beam model [19]. However, the best results found were restricted to a very short range of nominal value of tissue stiffness. Kobayashi et al. [15] developed a numerical simulation of a planning method using a liver-shaped 2D model. Their purpose was to develop a novel planning method to decide robust paths of straight needle insertion for various puncture points. Basically, they considered the puncture condition probabilistic and evaluated the expected value of needle placement accuracy. Experiments measuring needle placement accuracy showed that the method placed the needle with a mean accuracy of 1.5 mm.

Studies and observations of percutaneous insertions into elastic tissues have showed that the force data - collected from the needle insertion procedures - are a summation of stiffness, friction and cutting forces [20]. However, the energy of pure needle bending (transversal forces) dominates the total energy contribution to the system for insertions smaller than 90 mm [21]. Moreover, from their observations, it is possible to conclude that the energy stored in the system due to interaction of the tissue along to the needle shaft is very small for short insertions. Finally, they also showed that the energy associated to the bending due to axial load and compression at the tip are related to less than 0.1% of the total energy stored in the system, regardless of the insertion depth. Model's approximations proposed by our study concerning the friction and cutting forces are in accord to such observations. It will be discussed in the next section.

The main contribution of this work is to demonstrate the feasibility of merging needle-tissue properties, tip asymmetry and needle tip position updates to assist needle placement. Percutaneous needle insertion modeling is provided in order to reduce the needle's deflection prediction errors. The model is able to provide offline predictions. Additionally, online updates of the needle tip position support adaptive corrections. Experiment results reveal that such corrections have the potential to improve the model´s performance under uncertainties conditions such as tissue deformation, tissue inhomogeneity, needle-tissue friction, tissue's topological changes of the tissue and other modeling approximations. The system is evaluated by experiments in soft (homogeneous) PVC and multilayer tissue phantoms. Moreover, online and offline predictions were compared with trends in the empirical data. The method proposed in this work may provide promising support to applications such as tissue's entry point assistance, pre/intra-operative path planning and needle guidance.

II. METHODOLOGY

In this section, we go first through the biomechanics-based model and demonstrates how it provides offline needle bending predictions by relating stiffness and deflections of semi-rigid needle. The online needle deflection predictions and adaptive corrections are also presented. Secondly, we describe how qualitative tissue's properties measurements were estimated.

A. Adaptive Slope Model

Deflection (δx) of the semi-rigid needle when interacting with a soft tissue is modeled as a function of the needle (Kn) and tissue (Kt) properties (stiffness), as well as the needle tip asymmetry (α) and the insertion depth (δy). We assume that the semi-rigid needle deflects according to the small-deflection beam theory ($\delta x/L < 0.1$) [22] in the direction of the bevel due to the asymmetric forces acting on the needle tip (Fig. 1). L ($\theta \sim sin\theta$) is taken as the needle length (distance AB between the end-effector and the needle tip) projected along the y axis and δx is the needle tip deflection orthogonal to the insertion direction. Finally, the resultant force $\vec{F}_R$ represents the sum of all the forces actuating on the system, in particular the input force $\vec{F}$ and friction force $\vec{F}\mu$. The derived expressions concern the dynamics of the needle during the insertion into an elastic body and describe the relationship between the normal ($\vec{N}$) and the components of the resultant force ($\vec{F}_R$) acting on the needle as shown in Fig. 1.

The analysis takes Kt as the tissue stiffness at the needle tip, and assumes that the resultant force's component in the x axis ($\vec{F}_{Rx}$) is the same needed to compress parallel virtual springs, in which stiffness of each spring is given by the needle (Kn) and tissue (Kt) stiffness. The needle axial deformation is negligible compared to the tissue deformation. Therefore, the resulting y-component ($\vec{F}_{Ry}$) is represented by a single spring with stiffness Kt. This lead to:

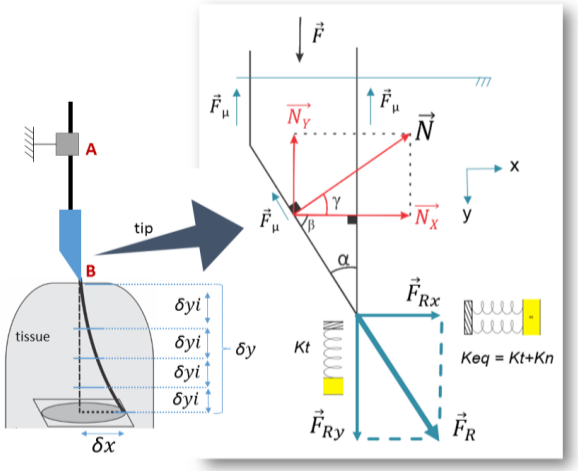

Fig. 1. Needle tip deflection modeling. Left: Needle deflections are assumed to be towards the direction of the bevel. Right: Study of the normal and resultant forces

$$\vec{F}_{Rx} = (Kn + Kt) * \delta x \quad (1)$$

and

$$\vec{F}_{Ry} = Kt * \delta y \quad (2).$$

In the relationship presented below (3), the system's dynamic analysis during the insertion is considered. $\vec{F}_{Rx}$ acts transversally and causes needle deflection, while $\vec{F}_{Ry}$ is the axial force that allows needle displacement in the y axis. Resultant forces in the transversal and axial directions are observed in the relationship with each component of the normal force acting in the same direction. The adaptive parameter (H) was conceived as the slope in the relationship between the axial and transversal components of the model. Its updates work as a failure contingence mechanism and allow online adaptive correction regarding to the error ($e_i = \delta x_i - \delta x'_i$) between the predicted deviation (δx_i) at the insertion step i and the needle tip deviation observed ($\delta x'_i$) from the image.

$$\vec{F}_{Rx}\Big/\vec{N}_x = \vec{F}_{Ry}\Big/-\vec{N}_y * H \quad (3)$$

Therefore, using (5), H is updated for each insertion step (4), according to the needle tip position tracked in the images. The update, for each insertion step i, is performed according to

$$H_i = H_{i-1}(\delta x_i + e_i). \quad (4)$$

Being that the deflection prediction for the next insertion step δx(i+1) is performed considering the current needle tip update H(i) at the time i. The study of the normal force in the needle tip (Fig. 1), shows that the angle γ is the same one as in the beveled needle tip (γ = α). Then, having $\vec{N}x = cos(\alpha) * \vec{N}$ and $\vec{N}y = sin(\alpha) * \vec{N}$ and from (1), (2) and (3), we can write the needle tip deflection for the x direction as:

$$\delta x = \sum_{i=1} \frac{cot(\alpha) * Kt_{i-1} * \delta y_i * H_{i-1}}{Kt_{i-1} + Kn} \quad (5)$$

Despite the model is presented in 2D, it can be easily extended to 3D. During the training experiments, a set of previous observations [23] of δx of a semi-rigid needle interacting with PVC and ex-vivo pork phantom tissues were used for the tuning of the initial H value (H_0). Using (5), H_0 was found to be nearly constant into the empiric data samples, presenting an average value of 0.02 and a pattern deviation of 0.004. The definition of H_0 is central to allow offline predictions. This initial value is invariant, regardless of the needle and tissue parametric changes through different experimental conditions.

As expected, H_0 is smaller than 1, because the transversal factor ($\frac{\vec{F}_{Rx}}{\vec{N}_x}$) in (3) tends to be much smaller than the axial factor ($\frac{\vec{F}_{Ry}}{-\vec{N}_y}$). This is due to the fact that the needle moves more axially than transversally. Both factors are considered to contain the parametric abstractions assumed to influence needle deflection: needle tip asymmetry, tissue and needle stiffness, insertion depth and resultant forces (virtual springs). Therefore, if the most important parameters provoking needle deflection are contained in the model's factors, the approximations with less significant meaning - represented by H - should express little variation under short insertions. It can be confirmed by the very low pattern deviation of H_0. Such observation is also in accord with the observations of Misra et al. [21], in which pure needle bending energy is showed to be the only energy with significant value in the system for the initial insertion depths (<40 mm). Once H_0 is computed, the compensation of the model's approximations is performed recursively. The position-based updates are proposed to overcome approximation errors, such as friction along the needle shaft, tissue's topological changes or input measurement errors. E.g., some of the experiments evaluate the behavior of the model in the special case of multi-layer tissues, for which only superficial tissue properties measurements of Kt is known. This special case could be particularly interesting when facing a future scenario of needle placement into biological or in-vivo tissues, where no elastography or force sensor input is available intra-operatively (online). Results obtained from experiments reveal potential to overcome the initial measurement inaccuracy regarding the heterogeneity and inhomogeneity of tissue's parameters.

B. *Qualitative tissue properties measurements*

The qualitative properties of the tissue (stiffness) at surface level are estimated using adaptation based on the experiment described in [7]. It will be described following. For the experiments, long (20 cm), Stainless (316) steel, 18-gauge, 17 degrees bevel-tip needle was used having an outer diameter (do) of 1.27 mm and an inside diameter (di) of 0.838 mm. It exhibits 193-GPa Young modulus (E) [7] and moment of inertia $I = \pi/64 * (do^4 - di^4)$ = 0.103 mm^4. The needle stiffness is given by $Kn = 3EI/L^3$, L being the needle length. The stiffness coefficient at the tissue's surface level is estimated by measuring force and axial displacement of the needle tip for short insertions (δy = 5 mm depth) while touching the tissue (Fig. 2). Robot's encoders were used to obtain δy. Since elastic modulus changes is as a function of

strain, the coefficient of the virtual spring is updated according to the strain-dependent dynamic elastic modulus. As the shape of the tissue's surface changes, the location and orientation of the virtual spring change accordingly. According to [7], the local stiffness parameter is an important spring coefficient that expresses the force of the tissue on the needle as a function of local displacement. Therefore, the force F applied by a virtual spring is proportional to the displacement of the spring from its initial position δy =(y - y0).

$$F = -Kt * (y - y_0) \quad (6)$$

III. Results

In this section, we present the experimental setup used to predict needle deflections into elastic phantom tissues, experimental cases and prediction results.

A. Experimental Setup

Experiments were performed using a robot-driven needle interacting with different phantom tissues and using the (6 DoF + grasp) cable-driven Raven II robot platform [24]. For the experiments, the robot tools were removed and a customized adapter was built in order to fix the base of the needle and the force sensor in the robot's arm (Fig. 3). The 6-DoF force-torque sensor (nano43 / SI-36-0.5 / ATI Industrial Automation) was used for the surface compression tests only once and before start the experiment (pre-operatively). The insertion experiments were performed without considering the force sensor data input during the insertions (intra-operatively). The robot was commanded by a teleoperation platform (UDP protocol), having the 7-Dof Sigma.7 (ForceDimension) working as haptic master device (Fig. 2B). A Graphical User Interface (GUI) was developed in order to supply online image feedback and procedure data, such as target's depth, current needle-target's distance and needle path, including its estimated error. Video images (1920 x 1080 px) were acquired using a digital video camera Toshiba Camileo Z100 and measurements of the scenario were recovered thanks to accurate camera calibration using planar fiducials markers [25].

The needle was visually detectable because the tissues used were translucent. The track of the needle's position was performed manually. It was done by using a single mouse's click in the interactive GUI. The insertions were performed under iterative-time [26], i.e., progressively, with regular intervals after insertion steps.

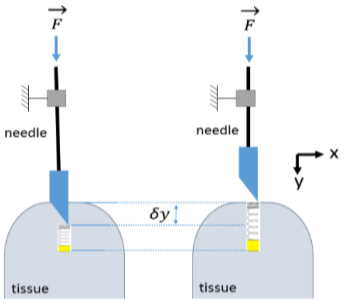

Fig. 2. Qualitative tissue stiffness measurement.

Each insertion step had around 3 cm of depth. During the intervals (around 5 seconds), the user was allowed to update the current needle tip. The needle tip position updates were used to provide adaptive corrections to the previous needle deflection prediction. The needle insertion velocity was of 0.06 m/s and the depth range between 50 and 100 mm. Pre-operative parameters such as needle and tissue properties were obtained once, at tissue's surface level, without further online updates.

B. Experimental Cases

Three experimental cases were used to evaluate the modeling under situations involving different puncture conditions. Elastic tissue phantoms prepared for each experimental case is presented in Fig. 4. The experimental cases are:

a) Case 1 (Homogeneous tissue): The needle is inserted into the 100% soft (homogeneous) PVC phantom towards a target defined offline.

b) Case 2 (Two-layers phantom): The needle is inserted into the two-layers phantom. The phantom's layers are composed by i: soft PVC; ii) extra soft PVC (80% soft PVC + 20% softener).

c) Case 3 (Four-layers phantom): The needle is inserted through the four-layers phantom. The phantom's layers are composed by synthetic leather, spongy tissue, soft and hard PVC. This phantom intended synthetically to reproduce the multi-layer medium often found in the clinical procedures, such as skin, fat, mussels and organ.

The target is defined offline. Online adaptive corrections are provided to improve the needle tip deflection prediction in the end of the procedure. The tissues properties were preoperatively estimated at tissue surface level using axial axial compression test as previously described in the methods.

C. Experimental Results

Insertion depths were observed inside the range of 6 and 10 cm. Ten to twenty insertions were performed for each experimental case with constant velocity of 3 m/s. Overall, 41 insertions were performed.

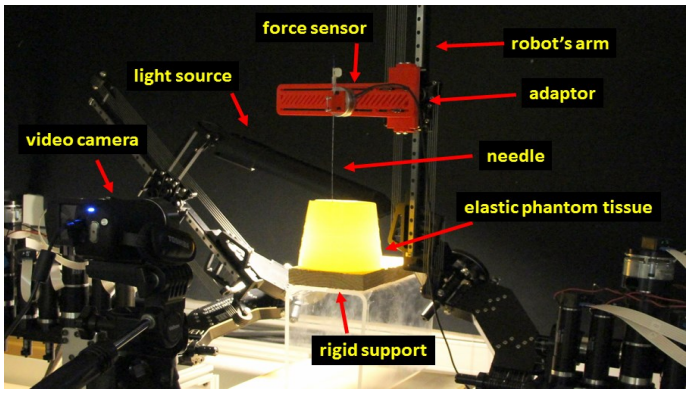

Fig. 3. The Raven II platform. Original architecture was customized in order to perform needle insertion experiment.

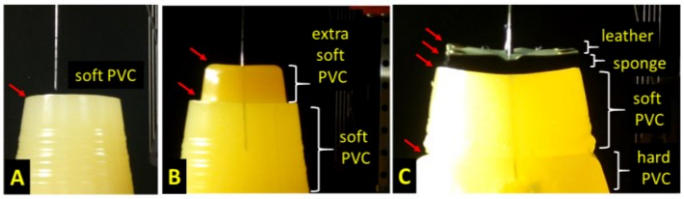

Fig. 4. Elastic tissue phantoms prepared for each experimental case. A. Homogeneous soft PVC. B. Two-layers phantom. C. Four-layers phantom. Layer's edge are indicated by red narrows.

The needle insertion procedure stopped when the tracked needle tip and the target's depth were the same. The average prediction error and standard deviation for 20 experiments of Case 1 is 0.78 $\pm$ 0.39 mm. Case 2 showed an average of needle deflection prediction error of 0.93 $\pm$ 0.36 mm, considering 10 needle insertions samples. The 11 insertions samples performed in the Case 3, the needle deflection prediction error was of 1.42 $\pm$ 0.74 mm when inserted into four-layer phantom tissue (Table 1).

TABLE I. NEEDLE DEFLECTION PREDICTION AVERAGE ERROR.

Experimental case	Prediction error and standard deviation	Number of insertions
Case 1	0.78 ± 0.39 mm	20
Case 2	0.93 ± 0.36 mm	10
Case 3	1.42 ± 0.74 mm	11

The error is calculated as the Euclidean distance between the desired target position and the needle tip position measured using the manual tracking. Results showed in the Case 3 could be tolerated by most of surgical needle placement procedures. Fig. 5 shows a sample of needle insertion procedure performed in Case 1. The target is situated at 76 mm depth (Fig. 5A). The offline needle deflection prediction allows to define the best entry point. In this case, the predicted deflection was of 4.37 mm when compared to a linear referential (Fig. 5B). The sequential insertion steps are followed by updates of needle tip position, measured by manual tracking using the interactive GUI (Fig. 5C-G).

The Fig. 5H shows that, for this sample, the final needle deflection matched the predicted one. It is possible to observe that the needle shaft presents significant movements inside the tissue during the insertion procedure. For example, the fixed fiducial point in the Fig. 5C is completely misaligned to the shaft position in the Fig. 5G. It happens mainly because the needle bending outside the tissue may also be a source of interference in the needle trajectory. Nevertheless, over all the three experimental cases, the difference between the error of the offline predictions and the prediction errors after adaptive corrections reveals error decreasing of 25%.

The evolution of the needle deflection as a function of the insertion depth for all the samples is showed in Fig. 6. The final measured needle tip position (N) was plotted for each one of the three cases, as well as the predictions performed pre-operatively (offline) and online, respectively (P) and (O).

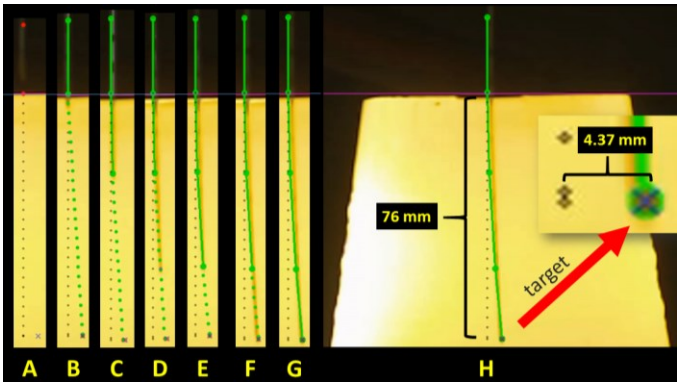

Fig. 5. Sequential insertion of semi-rigid needle into soft PVC Phantom tissue. The target is defined online (A), followed of offline needle deflection prediction (B). A loop of insertions and needle tip updates are performed (C-F) until the needle tip reaches the target depth (G-H).

It is possible to notice larger needle deviations in Case 1. Greater stiffness values on the tissue´s surface may increase needle bending outside the tissue and increase needle deflection. Moreover, numerous insertions in the same entry point region could release changes in the tissue´s topologies. It could reduce the outside tissue needle´s bending, as well as the needle deflection inside the tissue. The predictions could follow the needle deflections trends, while showing promising adaptive performance along to the three Cases. The results of the needle deflection prediction demonstrate that: a) offline predictions may be very useful to assist the user in the needle insertion point definition. b) Adaptive online corrections of the initial predictions show potential to overcome the models approximations and uncertainties of the scenario. c) Adaptive online corrections of initial predictions could be central to anticipate decisions of the user along to the insertion procedure. For example, by detecting changes in the path before the needle reach some important structure critical to the treatment or therapy.

IV. DISCUSSION

Our work was focused on the development of a novel method to assist robotic-drive placements of semi-rigid needle into elastic tissues. The model combines needle-tissue properties, tip asymmetry and updates of needle tip position in order to provide offline and online predictions of needle tip deflections as a function of the insertion depth. The approach is based on an adaptive slope parameter whose updates work as a failure contingence mechanism and allows online adaptive correction regarding to the error between the predicted observed needle tip deviations.

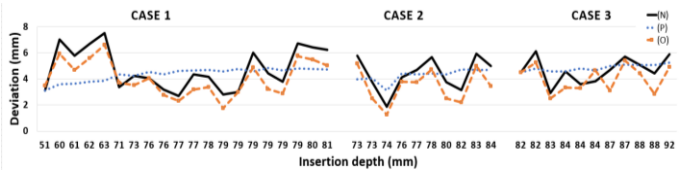

Fig. 6. Measures of needle's deflection (N) VS insertion depth for all the three Cases. Online and offline (pre-operative) deflections estimations are plotted, respectively, as (O) and (P).

Results demonstrate the potential of the approach to improve the model's performance under uncertainties conditions such as tissue deformation, tissue inhomogeneity, needle-tissue friction, topological changes of the tissue and other modeling approximations. Experiments were performed to evaluate the accuracy and needle tip deflection prediction of the proposed model. Online corrections improved offline predictions in the order of 25%, while needle placement over all the three cases presented an average error of 1.04 mm. Similar experiments were performed by Kobayashi *et al.* [15] with needle placement mean accuracy of 1.5 mm. In [8], curvature error average in gel was of 22.2% against the deviation average of 17.7% observed through the three cases of our work. Although the experimental conditions are not the same, it is interesting to notice that the errors achieved by these works were significantly higher than the errors presented in this study.

For simplicity's sake, a force sensor device was used in order to obtain the tissues' parameters offline. Moreover, the results obtained in this study are related to the measurement of Kt in the surface of the tissue performed only once and before starting the procedure (offline). After that, no input force measurements or updates of Kt is performed and all the adaptive compensations are based on the online position updates of the needle tip. Optionally, Kt could be measured preoperatively by using others tools, such as MRI elastography or Acoustic Radiation Force Impulse (ARFI).

A planning method to be developed will consider the effect of lateral movements in the base of the needle in order to steers its planned path. In addition, needle placement will be further verified by using ex-vivo tissue phantoms, taking into consideration obstacle avoidance and target displacements. Additionally, future works could investigate how online updates of Kt would impact the performance of the model. Techniques as elastography could support the pre-operative construction of a 3D stiffness map that could be used as online input source of Kt parameter, according to the current needle tip position updates. Such stiffness map could be registered to the scenario in order to provide Kt intermediate inputs. It could be very helpful concerning the tissue's heterogeneities and inhomogeneities. Our study has demonstrated the feasibility and advantages of combining needle-tissue properties, tip asymmetry and needle tip position updates to assist needle placement.

ACKNOWLEDGMENT

We thank Abdulrahman Albakri and Kilian Demeulemeester (LIRMM) for the support during the validation experiments using Raven II and revision of the work.

REFERENCES

[1] C. K. Chui, S. H. Teoh, C. J. Ong, J. H. Anderson and I. Sakuma, "Integrative modeling of liver organ for simulation of flexible needle insertion," in 9th International Conference on Control, Automation, Robotics and Vision - ICARCV, Singapore, 2006.

[2] D. Stoianovici, D. Song, D. Petrisor, D. Ursu, D. Mazilu, M. Mutener, M. Schar and A. Patricu, "MRI stealth robot for prostate interventions," Minimally Invasive Therapy & Allied Technologies, vol. 16, no. 4, pp. 241-248, 2007.

[3] R. J. Webster, N. J. Cowwan, G. S. Chirikjian and A. M. Okamura, "Nonholonomic modeling of needle steering," Int. Journal of Robotic Research, vol. 25, pp. 509-525, 2006.

[4] N. Abolhassani, R. Patel and F. Ayazi, "Effects of different insertion methods on reducing needle deflection," in Conf. Proc. of the 29th IEEE Engineering in Medicine and Biology Society Conference, Lyon, 2007.

[5] H. Su, M. Zervas , G. Cole, C. Furlong and G. Fischer, "Real-time MRI-guided needle placement robot with integrated fiber optic force sensing," in International Conference on Robotics and Automation (ICRA), 2011.

[6] S. P. DiMaio and S. E. Salcudean, "Needle Steering and Motion Planning in Soft Tissues," 2004.

[7] D. Glozman and M. Shoham, "Image-Guided Robotic Flexible Needle Steering," in IEEE Transactions on Robotics, Vol 23, N.03, 2007.

[8] Misra, S, K B Reed, B W Schafer, K T Ramesh, and A M Okamura. 2010. "Mechanics of flexible needles robotically steered through soft tissue." The International Journal of Robotics Research 29(13) 1640-60.

[9] D. S. Minhas, J. A. Engh, M. M. Fenske and C. N. Riviere, "Modeling of needle steering via duty-cycled spinning," in IEEE EMBS - Eng Med Biol Soc, 2007.

[10] D. C. Rucker, J. Das, H. B. Gilbert, P. J. Swaney, M. Miga, N. Sarkar and R. J. Webster , "Sliding model control of steerable needles," IEEE Trans on Robotics, vol. 29, no. 5, pp. 1289-1299, 2013.

[11] P. Moreira and S. Misra, "Biomechanics-based curvature estimation for ultrasound-guided flexible needle steering in biological tissue," Annals of Biomedical Engineering, 2014.

[12] J. Engh, G. Podnar, D. Kondziolka and C. Riviere, "Toward effective needle steering in brain tissue," EMBS Anual International Conference, pp. 559-562, 2006.

[13] B. Meiklejohn, "The effect of an epidural needle. An in vitro study," Anaesthesia, pp. 42(11):1180-2, 1987.

[14] R. Seifabadi, I. Iordachita and G. Fichtinger, "Design of a teleoperated needle steering system for MRI-guided prostate interventions," in Proc. of the Biomedical Robotics and Biomechatronics (BioRob), Rome, 2012.

[15] Y. Kobayashi, A. Onishi, H. Watanabe, T. Hoshi, K. Kawamura and M. G. Fujie, "Developing a Planning Method for Straight Needle Insertion using Probability-Based Condition where a Puncture Occurs," in IEEE International Conference on Robotics and Automation (ICRA), Kobe, Japan, 2009.

[16] E. Dehghan and S. Salcudean, "Needle Insertion Point and Orientation Optimization in Non-linear Tissue with Application to Brachytherapy," in IEEE International Conference on Robotics and Automation (ICRA), Roma, Italy, 2007.

[17] O. Goksel, S. Salcudean, S. DiMaio, R. rohling and J. Morris, "3D needle-tissue interaction simulation for prostate brachytherapy," Medical Image Computing and Conference on Robotics and Automation, pp. 827-834, 2005.

[18] N. Abolhassani and R. V. Patel, "Deflection of a Flexible Needle During Insertion into Soft Tissue," in Conf Proc IEEE Eng Med Biol Soc, New York City, USA, 2006.

[19] R. J. Roesthuis, Y. R. van Veen, A. Jahya and S. Misra, "Mechanics of Needle-tissue Interaction," San Francisco, CA, USA, 2011.

[20] A. Okamura, C. Simone and M. D. O´Leary, "Force modeling for needle insertion into soft tissue," IEEE Transactions on Biomedical Engineering, vol. 51, no. 10, pp. 1707-1716, 2004.

[21] S. Misra, K. B. Reed, B. W. Shafer, K. T. Ramesh and A. M. Okamura, "Observations and Models for Needle-Tissue Interactions," in Conf Proc IEEE Eng Med Biol Soc, Kobe, Japan, 2009.

[22] S. Timoshenko and J. Gere, Mechanics of materials, New York: Van Nostrand Reinhold Co., 1972.

[23] E. Dorileo, N. Zemiti, P. Poignet, N. Hungr, I. Bricault and C. Fouard, "Observations of lightly-flexible needle deflection in 3D CT/MRI," in Surgetica, Chambery le Menage, 2014 .